



Surface Structure Characterization of Shape and Size Controlled Pd Nanoparticles by Cu UPD: A Quantitative Approach

Emmanuel Garnier, Francisco J. Vidal-Iglesias, Juan M. Feliu and José Solla-Gullón*

Instituto de Electroquímica, Universidad de Alicante, Alicante, Spain

The search for new surface sensitive probes that characterize the surface structure of shape and size-controlled nanoparticles is an interesting topic to properly understand the correlations between electrocatalytic properties and surface structure at the nanoscale. Herein, we report the use of Cu UPD to characterize, not only qualitatively but also quantitatively, the surface structure of different Pd nanoparticles with controlled particle shape and size. Thus, Pd nanoparticles with cubic, octahedral and rhombic dodecahedral shapes, that is, with preferential {100}, {111}, and {110} surface structures, respectively, were prepared. In addition, cubic Pd nanoparticles with different particles sizes and spherical (2–3 nm) Pd nanoparticles were also synthesized. Based on the Cu UPD results on Pd single crystals, a new approach is proposed to qualitatively and quantitatively determine the percentages of {100}, {111}, and {110} surface domains present at the surface of the different shape and size controlled Pd nanoparticles. The results reported clearly show the benefits of this Cu UPD to get detailed information of the surface structure of the nanoparticles according to their particle shape and size.

Keywords: nanoparticles, shape, size, surface structure, electrocatalysis, Cu UPD

OPEN ACCESS

Edited by:

Vito Di Noto,
University of Padova, Italy

Reviewed by:

Dan Buttry,
Arizona State University, United States
Anthony Peter O'Mullane,
Queensland University of
Technology, Australia

*Correspondence:

José Solla-Gullón
jose.solla@ua.es

Specialty section:

This article was submitted to
Electrochemistry,
a section of the journal
Frontiers in Chemistry

Received: 24 May 2019

Accepted: 11 July 2019

Published: 31 July 2019

Citation:

Garnier E, Vidal-Iglesias FJ, Feliu JM
and Solla-Gullón J (2019) Surface
Structure Characterization of Shape
and Size Controlled Pd Nanoparticles
by Cu UPD: A Quantitative Approach.
Front. Chem. 7:527.
doi: 10.3389/fchem.2019.00527

INTRODUCTION

The surface structure of a metal plays a key role on its electrocatalytic properties. This is well-established thanks to the extensive and intensive studies performed with metal single crystal electrodes for most of the electrocatalytic reactions of interest (Korzeniewski et al., 2012). In addition, this surface structure sensitivity has been also reported to be of outstanding relevance for nanoparticulated metal materials, particularly from the availability of shaped metal nanoparticles and their application in Electrocatalysis (Solla-Gullón et al., 2006, 2008b; Solla-Gullón et al., 2011; Tian et al., 2007; Erikson et al., 2011, 2016a; Shao et al., 2011b; Jin et al., 2012; Vidal-Iglesias et al., 2012; Figueiredo et al., 2013). Accordingly, it is widely accepted that by controlling the shape of the nanoparticles, nanoparticles with a well-defined surface structure, that is, well-defined surface atomic arrangement and coordination, can be obtained (Tian et al., 2008; Zhou et al., 2009). Similarly, as reported in previous literature (Kinoshita, 1990; Shao et al., 2011a), when changing the particle size the surface structure of these sized-controlled metal nanoparticles is also strongly affected. In this way, it is highly important to develop sensitive probes to characterize the surface structure of these materials, in order to subsequently establish correct relationships between the surface structure and electrocatalytic reactivity at the nanoscale.

Among others, the use of pure electrochemical probes has been shown to be a powerful technique to successfully characterize the surface structure of different types of shape-controlled metal nanoparticles (Solla-Gullón et al., 2004, 2008a; Chen et al., 2012; Farias and Feliu, 2019; García-Cruz et al., 2019; Mayet et al., 2019). In addition, it is worth noting that this electrochemical surface structure characterization is (i) statistically representative, because thousands of nanoparticles are measured simultaneously, and (ii) performed in a similar environment than those that will be employed during the electrochemical reactions. Thus, for instance, in the case of platinum, the so-called hydrogen and anion adsorption/desorption region as well as the adsorption of bismuth and germanium adatoms have clearly shown the benefits of the electrochemical approach to gain relevant and very detailed information about the surface structure of the different shaped Pt nanoparticles (Solla-Gullón et al., 2004, 2008a; Rodríguez et al., 2005). Similarly, for gold surfaces, the underpotential deposition (UPD) of Pb has been shown to be an excellent probe for obtaining an estimation of the different surface domains present on various types of Au nanoparticles (Hernández et al., 2009; Chen et al., 2017; Jeyabharathi et al., 2018; García-Cruz et al., 2019). However, in the case of palladium, and despite some preliminary attempts (Jin et al., 2012; Solla-Gullón et al., 2015; Higuchi et al., 2018), a systematic analysis to qualitatively and quantitatively determine the presence of well-defined surface domains at the surface of different shape and size controlled Pd nanoparticles is still missing. This analysis will be based on the Cu UPD process on Pd which was reported to be highly sensitive to the surface structure as previously illustrated with Pd single crystal surfaces (Chierchie and Mayer, 1988; Cuesta et al., 1999; Vidal-Iglesias et al., 2006, 2007; Korzeniewski et al., 2012; Mayet et al., 2019).

A detailed characterization of the surface structure of the shape and size of controlled Pd nanoparticles will importantly help to provide better comprehension of the interesting electrocatalytic properties of these Pd nanomaterials toward relevant electrochemical reactions. This includes the oxygen reduction (Erikson et al., 2011, 2016a,b; Shao et al., 2011b, 2013a; Zhang et al., 2013), oxidation of some small organic molecules (Zhang et al., 2011; Jin et al., 2012; Vidal-Iglesias et al., 2012; Arjona et al., 2013; Kannan et al., 2013; Shao et al., 2013a; Chen et al., 2014; Yu et al., 2019), and CO₂ reduction (Klinkova et al., 2016; Huang et al., 2017; Gao et al., 2018) among others, because the surface structure of the nanoparticles, rather than the shape or size, is the key point determining the resulting electrocatalytic activity (obviously, the atomic composition is also extremely relevant). Consequently, the aim of this manuscript is to develop an electrochemical approach, based on the Cu UPD reaction of Pd, to quantify the percentage of {100}, {110}, and {111} surface domains on different shape and size-controlled Pt nanoparticles.

MATERIALS AND METHODS

Synthesis of Nanoparticles

The different Pd nanoparticles used in the present manuscript were prepared using some previously described methodologies.

Shape-controlled, including cubic (Pd_{Cub}), octahedral (Pd_{Oct}), and rhombic dodecahedral (Pd_{RD}) Pd nanoparticles, ideally enclosed by {100}, {111}, and {110} facets, respectively, were obtained using a seed-mediated method (Niu et al., 2010). In brief, this methodology is based on the growth of Pd nanocubes (~20 nm) which act as seeds, in the presence of L-ascorbic acid (AA), H₂PdCl₄, cetyltrimethylammonium bromide (CTAB), and NaI as a reducing agent, Pd precursor, capping agent, and additive, respectively, at a specific reaction temperature during a particular reaction time. By controlling some of these experimental parameters, different shapes can be obtained. **Table 1** summarizes the experiment parameters used for each case. In a typical synthesis, the required amount of NaI solution was added to 25 mL of a 100 mM CTAB solution at a given temperature (in an oil bath). Then, 625 μL of a 10 mM H₂PdCl₄ solution and 200 μL of the ~20 nm as-synthesized seed Pd nanocube solution were added. Finally, a given volume of a freshly prepared 100 mM ascorbic acid solution was added and thoroughly mixed. This final solution was kept at the designated temperature during the required reaction time. The reaction was stopped by centrifugation (6,000 rpm, 10 min) and samples were twice centrifuged and dispersed in water. As described in previous contributions, an additional alkaline cleaning step is needed (Erikson et al., 2011; Montiel et al., 2017). A NaOH pellet was added to the water solution containing the nanoparticles. The incorporation of the NaOH produces the destabilization of the nanoparticles which precipitate. After complete precipitation, the nanoparticles were washed 3–4 times with ultrapure water (Milli-Q) and finally stored in a water suspension.

To evaluate the effect of the particle size, and based on previous literature (Niu et al., 2008; Lim et al., 2010; Erikson et al., 2016a), different size-controlled Pd nanocubes (~20 and ~10 nm) were also prepared. In both cases, the synthesis is based on a one-step approach. Very briefly, for the preparation of ~20 nm Pd nanocubes (these Pd nanocubes are the ones used as seeds for the seed-mediated method described above, Pd²⁰_{Cub}), 10 mL of 10 mM H₂PdCl₄ and 200 mL of 12.5 mM CTAB were mixed together and placed in an oil bath at 95 °C for 5 min. Then, 1.6 mL of a 100 mM ascorbic acid solution was incorporated and the reaction was allowed to proceed for 30 min at 95 °C. After the solution had cooled down, the solution was twice centrifuged and dispersed in water. Finally, a NaOH pellet was added to this solution. Once the nanoparticles were completely

TABLE 1 | Summary of the experimental conditions for the growth of cubic (Pd_{Cub}), octahedral (Pd_{Oct}), and rhombic dodecahedral (Pd_{RD}) Pd nanoparticles at a controlled temperature (T) during *t* hours.

	T/K t/h	NaI	CTAB	H ₂ PdCl ₄	Seeds	Ascorbic acid
Pd _{Cub}	328 K	25 μL	25 mL	625 μL	200 μL	100 mM
	4.5 h	0.1 mM	100 mM	10 mM		250 μL
Pd _{Oct}	313 K	125 μL	25 mL	625 μL	200 μL	100 mM
	15 h	1 mM	100 mM	10 mM		250 μL
Pd _{RD}	353 K	125 μL	25 mL	625 μL	200 μL	100 mM
	1 h	1 mM	100 mM	10 mM		500 μL

precipitate, they were washed 3–4 times with ultrapure water and finally stored in a water suspension. For the synthesis of the ~ 10 nm Pd nanocubes ($\text{Pd}^{10}_{\text{Cub}}$), 11 mL of an aqueous solution containing given amounts of PVP (MW $\approx 55\,000$, 105 mg), K_2PdCl_4 (57 mg), NaBr (300 mg) and ascorbic acid (60 mg) were mixed together in water and then heated for 3 h at 80°C . The cleaning of this sample was performed as suggested by Zalineeva et al. (2013, 2015) by the addition of NaOH pellets until having an ~ 1 M NaOH solution. Under these conditions, the nanoparticles precipitate which were finally washed 3–4 times with ultrapure water and finally stored in a water suspension. Finally, and for the sake of comparison, spherical (~ 3 nm) Pd nanoparticles (Pd^3_{Sp}) were also prepared using a previously published methodology (Vidal-Iglesias et al., 2012). Very briefly, 0.6 mL of an ice-cold and freshly prepared 0.1 M NaBH_4 solution was added to a 20 mL aqueous solution containing 2.5×10^{-4} M H_2PdCl_4 and 2.5×10^{-4} M trisodium citrate prepared in a glass beaker at room temperature. The resulting solution was vigorously stirred for 30 s and subsequently keep unperturbed for the next 30 min. Then, a NaOH pellet was directly added to the solution which results in the destabilization of the nanoparticles which slowly precipitate. Once precipitated, the sample was washed 3–4 times with ultrapure water and finally stored in a water suspension.

TEM experiments were performed with a JEOL JEM-2010 microscope working at 200 kV. Samples for TEM analyses were prepared by depositing a small droplet of the nanoparticle water suspension onto a formvar/carbon-coated copper grid.

The sample was then allowed to evaporate in the air at room temperature.

Electrochemical Characterization

The Pd samples were electrochemically characterized in a conventional three-electrode electrochemical cell at room temperature. An Autolab PGSTAT302N (Metrohm Autolab) system was used to control the electrode potential. Potentials were measured against a reversible hydrogen electrode connected to the cell through a Luggin capillary. A platinum wire was employed as a counter electrode. Working electrodes were prepared by mounting glassy carbon (GC) disks (3 mm diameter, Goodfellow) into Teflon holders. The surface of the electrodes was polished to a mirror finish with 1.0 and $0.3\ \mu\text{m}$ alumina slurries (Buehler). After polishing, the electrodes were sonicated in Milli-Q water (Millipore) in order to remove polishing residues. The catalyst ink (2–5 μL) was pipetted onto the GC electrode surface and the solvent was evaporated at room temperature in an Ar atmosphere.

Pd single crystal electrodes [Pd(111), Pd(100), and Pd(110)], ~ 2 mm in diameter, were manufactured using the Clavilier method (Clavilier et al., 1980; Hoshi et al., 2000). After the electrodes were flame annealed and cooled down, they were protected by a droplet of ultrapure water and transferred into the electrochemical cell.

The surface cleanness and surface structure of the Pd nanoparticles was evaluated in an Ar-saturated 0.1 M H_2SO_4

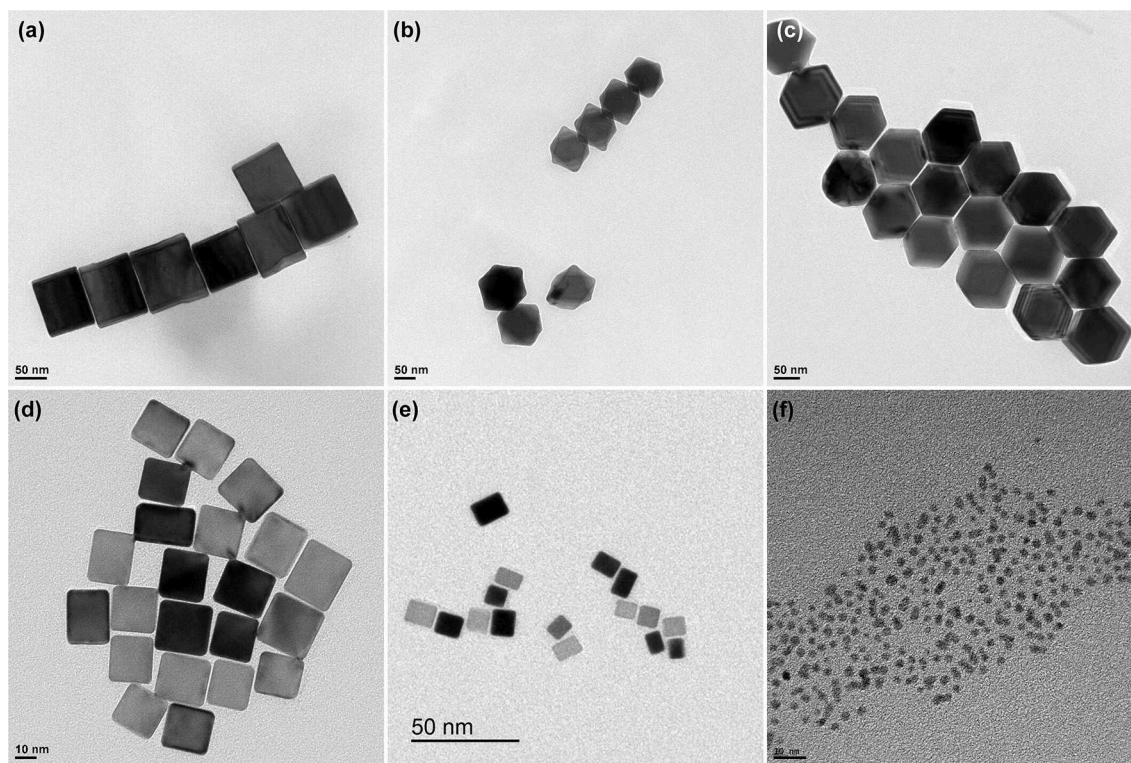


FIGURE 1 | Representative TEM images of the (a) Pd_{Cub} , (b) Pd_{Oct} , (c) Pd_{RD} , (d) $\text{Pd}^{20}_{\text{Cub}}$, (e) $\text{Pd}^{10}_{\text{Cub}}$, and (f) Pd^3_{Sp} nanoparticles.

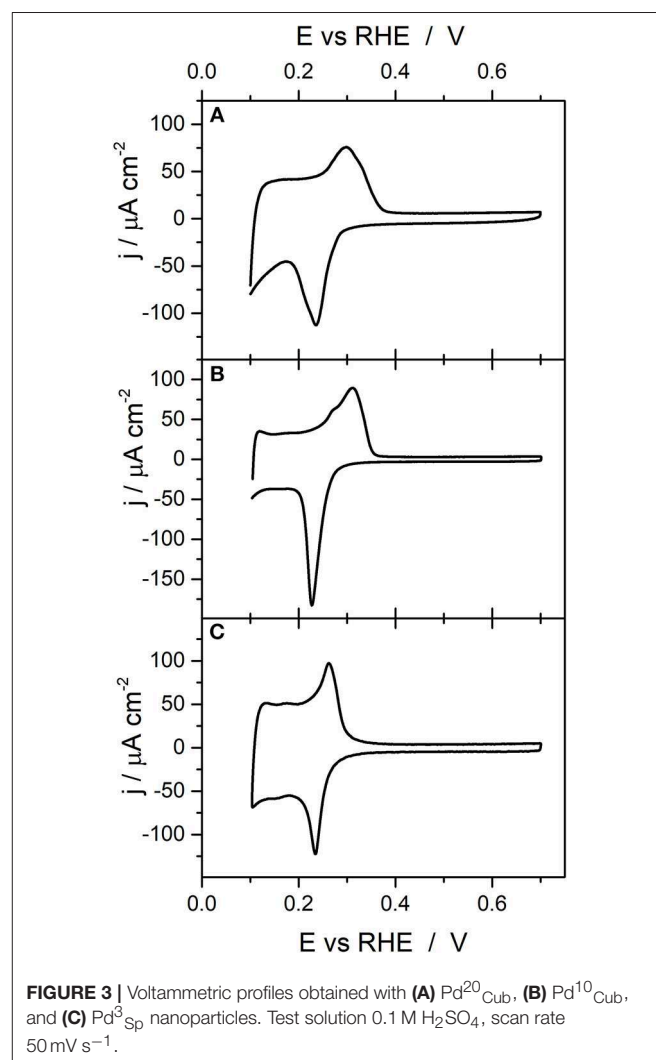
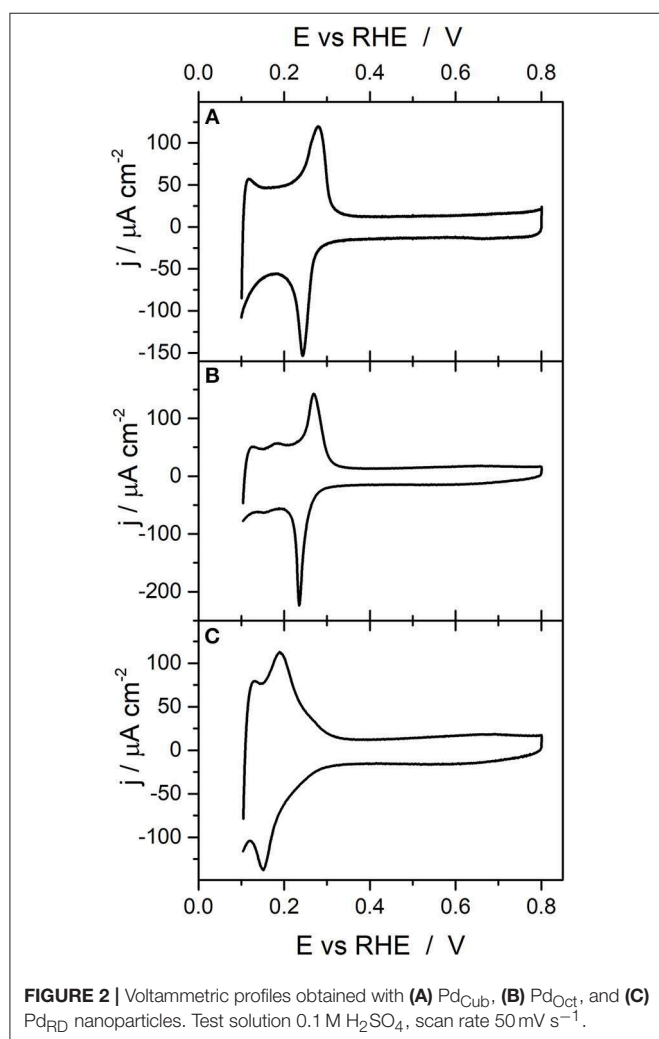
solution prepared from Millipore Milli-Q water and Merck 96% H_2SO_4 deaerated with Ar (99.99%, Air Liquide). For this purpose, the potential was recorded between 0.1 and 0.7 V at 50 mV s^{-1} , being the lower potential limited to 0.1 V to avoid hydrogen absorption. Then, to completely clean the surface of the samples, carbon monoxide (CO, 99.997% Air Liquide) was adsorbed onto the Pd catalyst (bubbling CO through the electrolyte at 0.1 V) until the surface was fully CO-covered (verified by cycling the electrode between 0.1 and 0.35 V). Once the surface was checked to be fully blocked, CO was removed from the solution by bubbling Ar (10–12 min for every minute CO was dosed to the solution). Finally, the CO monolayer was electrochemically stripped off from the surface of the Pd particles by sweeping the potential up to 1.0–1.1 V. The subsequent voltammogram corresponding to the CO-free surface was recorded afterwards, both to confirm the absence of CO in the solution and to have the voltammetric profile of the clean nanoparticles. With this latter curve, the active surface area of the Pd nanoparticles was determined with the charge involved in the so-called hydrogen underpotential deposition (UPD) region (between 0.10 and 0.60 V) assuming $212 \mu\text{C cm}^{-2}$

for the total charge, measured in H_2SO_4 , after the subtraction of the double-layer charging contribution (Woods, 1976).

Cu UPD experiments were performed in a 0.1 M H_2SO_4 + 1 mM CuSO_4 (Merck, p.a.) + 1 mM NaCl (Fluka, p.a.) solution. The electrode was immersed at a potential of 0.75 V and cycled until a lower potential limit of about 0.2–0.35 V, depending of the nature of each sample, to avoid bulk Cu deposition at the surface of the Pd nanocrystals (Solla-Gullon et al., 2015).

RESULTS AND DISCUSSION

Figure 1 displays some representative TEM images of the different Pd nanoparticles synthesized in this work. **Figures 1a–c** display the shaped Pd nanoparticles prepared using the seed-mediated approach (Niu et al., 2010). These TEM images show well-defined shapes associated with cubic, octahedral and rhombic dodecahedral Pd nanoparticles. It is worth noting that all nanoparticles appear well-separated which is a consequence of the residual presence of PVP or CTAB molecules surrounding the nanoparticles (TEM grids were prepared after centrifugation



of the samples and before the incorporation of NaOH). From a statistical analysis of the collected TEM images, we observed a high percentages of cubes (96.0%), octahedra (89.1%) and rhombic dodecahedra (93.3%). The particle size (size edge) of the cubes, octahedra, and rhombic dodecahedra was found to be about 81.2 ± 7.1 , 91.7 ± 8.5 and 51.8 ± 5.2 nm, respectively. The results are in good agreement with those previously reported by Niu et al. (2010). On the other hand, **Figures 1d,e** show the TEM images of the size controlled Pd nanocubes. The Pd nanocubes prepared in the presence of CTAB display a well-defined cubic shape, a high cubic yield (>90%) and a particle size (size edge) of 21.1 ± 3.0 nm. Similar results were obtained with those prepared in the presence of PVP which also show a well-defined cubic shape, a high cubic yield (>90%) but a smaller particle size (size edge) about 10.1 ± 1.7 nm. It is worth noting that, in these two cases, the preferential cubic shape is related to the interplay of bromide chemisorption on the seeds to promote the formation of {100} facets and an oxidative etching which removes the multiple-twinned seeds (Xiong and Xia, 2007; Xiong et al., 2007; Long et al., 2014). In both cases, the remaining fraction mostly consists of multiplied twinned nanoparticles like decahedra and icosahedra, right bipyramids, nanorods and undefined shapes. (Scardi et al., 2015; Solla-Gullon et al., 2015). Finally, **Figure 1f** shows the quasi-spherical Pd particles obtained in the presence of citrate which present a particle size (diameter) of about 2.8 ± 0.4 nm.

It is well-accepted that one of the most critical questions to correctly employ these nanomaterials in Electrocatalysis is regarding the cleanness of their surface. However, this important requirement is clearly faced with the need to use capping or surface-stabilizing agents to obtain shaped nanoparticles. Consequently, efficient decontamination protocols to completely remove these capping or surface-stabilizing agents from the surface of the nanoparticles are required (Montiel et al., 2017). Fortunately, as previously stated in the experimental section, the

NaOH chemical cleaning (alkaline treatment) has demonstrated to be very efficient for the removal of the capping agents here used (CTAB, PVP and citrate) (Erikson et al., 2011; Vidal-Iglesias et al., 2012; Zalineeva et al., 2013). In addition, as usual, an additional electrochemical cleaning with CO adsorption and its subsequent stripping was also carried out.

Figure 2 shows the voltammetric profiles in the so-called hydrogen/anion adsorption-desorption region obtained with the cubic, octahedral and rhombic dodecahedral Pd nanoparticles. In all cases the lower potential is limited to 0.1 V to avoid hydrogen absorption (Zalineeva et al., 2015). The reported voltammetric results are in good agreement with what is expected from previous single crystal studies (Hoshi et al., 2000, 2002; Wan et al., 2000; Hara et al., 2007). Thus, for the Pd_{Cub} nanoparticles (**Figure 2A**), anodic and cathodic contributions are observed at about 0.28 and 0.24 V, respectively. These voltammetric features are similar to those observed with Pd(100) and Pd(S)-[*n*(100)×(111)] and Pd(S)-[*n*(100)×(110)] electrodes (Hoshi et al., 2000, 2002; Hara et al., 2007). For the Pd_{Oct} nanoparticles (**Figure 2B**), the voltammetric profile also shows an anodic feature at 0.27 V and a sharp cathodic one at about 0.235 V, this sharp cathodic contribution being a characteristic feature of Pd(111), Pd(S)-[*n*(111)×(111)] and Pd(S)-[*n*(111)×(100)] electrodes (Hoshi et al., 2000, 2002; Hara et al., 2007). Finally, the voltammetric response of the Pd_{RD} nanoparticles does not show well-defined contributions although two broad peaks were observed at about 0.19 and 0.15 V. A similar poorly defined voltammetric feature was observed for Pd(110) electrodes and also for Pd(S)-[*n*(100)×(111)] and Pd(S)-[*n*(100)×(110)] electrodes with low *n* values (*n* = 2 and 3) and also for Pd(S)-[*n*(111)×(111)] and Pd(S)-[*n*(111)×(100)] electrodes also with low *n* values (*n* = 2 and 3) (Hoshi et al., 2000, 2002; Hara et al., 2007). All these findings point out that the cubic, octahedral and rhombic dodecahedral Pd nanoparticles present a preferential {100}, {111}, and {110} surface structure, respectively.

On the other hand, it is also worth mentioning that from the charge involved in this hydrogen/anion adsorption-desorption region, the electroactive surface area of the Pd sample can be easily estimated as previously described in the experimental section. A correct determination of the electroactive surface area is an indispensable point to properly compare the activity of different samples (Fang et al., 2010; Shao et al., 2013b; Moniri et al., 2017; Voiry et al., 2018).

Figure 3 reports the voltammetric profiles obtained with the ~20 nm and ~10 nm cubic Pd nanoparticles as well as that obtained with the quasi-spherical (~3 nm) Pd nanoparticles. The voltammogram obtained with the Pd_{Cub}²⁰ nanoparticles is

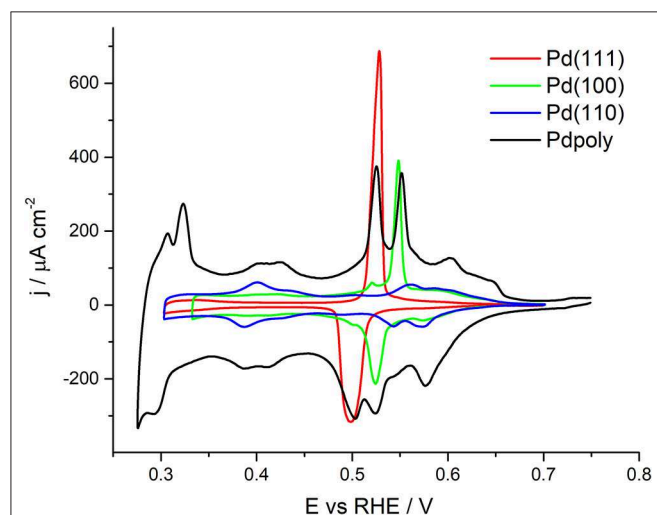


FIGURE 4 | Cu UPD voltammograms obtained with the three Pd single crystal basal planes and with a polyoriented Pd electrode. Test solution 0.1 M H₂SO₄ + 1 mM Cu²⁺ + 1 mM NaCl, scan rate 50 mV s⁻¹.

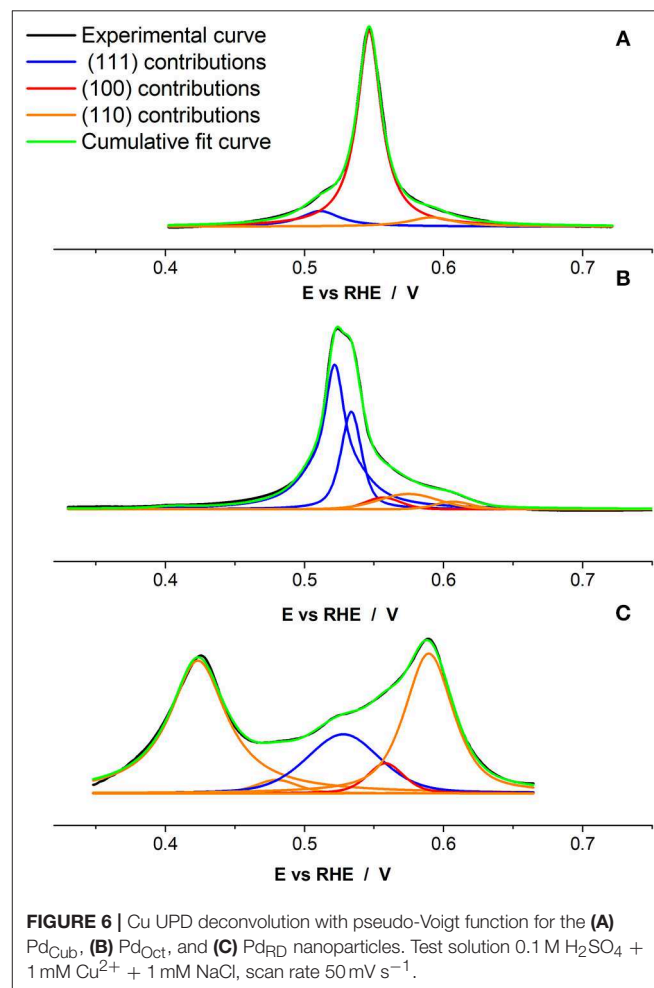
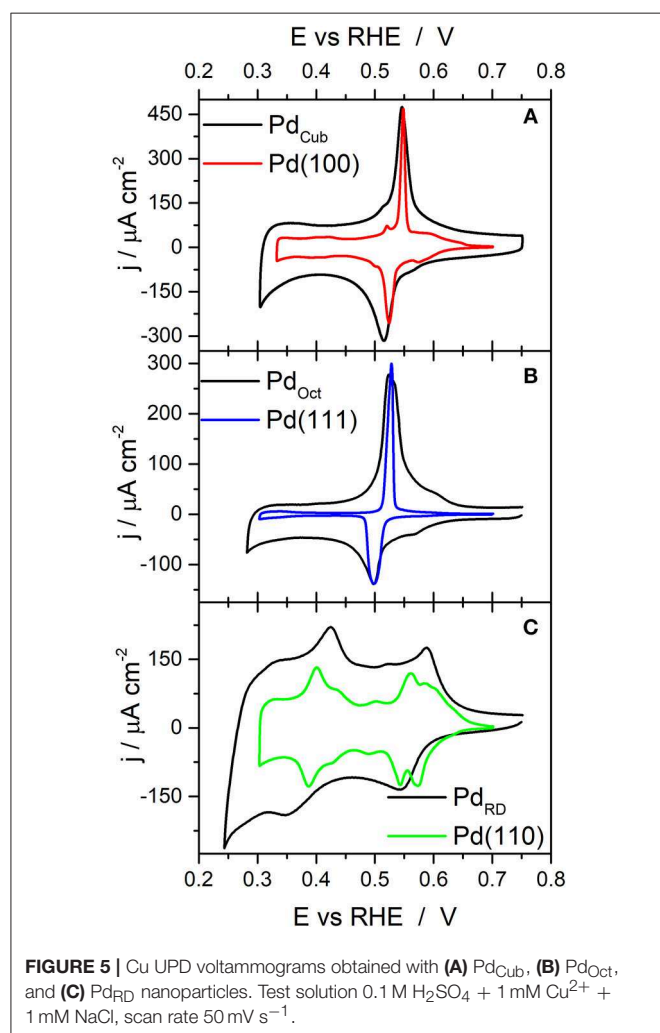
TABLE 2 | Peak potential and full width at half maximum for the main Cu UPD contributions observed in **Figure 4** for the three Pd basal plane electrodes.

Surface	Main peak/V	FWHM/mV
Pd(111)	0.529	10
Pd(100)	0.548	7
Pd(110)	0.587 and 0.606	25 and 54

similar to that observed in previous contributions with similar samples (Erikson et al., 2011; Vidal-Iglesias et al., 2012; Solla-Gullon et al., 2015) and displays voltammetric features associated with a preferential {100} surface structure. In particular, the voltammogram presents an anodic broad peak centered at about 0.296 V and a cathodic one at about 0.236 V. The presence of broader peaks in comparison with the Pd_{Cub} sample (~80 nm) suggests the existence of a less uniform distribution of {100} domains and/or a higher contribution of other surface sites. A similar trend is also observed with the Pd¹⁰_{Cub} nanoparticles. However, in this case, the cathodic contribution is clearly sharper than that obtained with the Pd_{Cub} (~80 nm) and Pd²⁰_{Cub} nanoparticles, which suggests the presence of a higher contribution of {111} surface domains. Finally, the voltammetric response of the quasi-spherical (~3 nm) Pd nanoparticles is similar to that characteristic of a polyoriented Pd surface (Burke and Nagle, 1999; Vidal-Iglesias et al., 2012).

From the voltammetric responses shown in Figures 2, 3, it is possible to infer some qualitative information about the surface structure of the different shape and size-controlled Pd nanoparticles. However, it would highly desirable to have some

electrochemical surface probe to quantitatively evaluate the surface structure of these nanoparticles. In this sense, Cu UPD on Pd is an interesting process because it has been reported to be sensitive to the surface structure of the Pd electrodes (Chierchie and Mayer, 1988; Cuesta et al., 1999; Herrero et al., 2001; Vidal-Iglesias et al., 2006; Mayet et al., 2019). To evaluate this surface structure sensitivity, Figure 4 shows the Cu UPD profiles obtained in a 0.1 M H₂SO₄ + 1 mM CuSO₄ + 1 mM NaCl solution with the three Pd basal planes (Pd(111), Pd(100), and Pd(110)) and with a polyoriented Pd bead. In all cases the lower potential limit is limited exclusively to the Cu UPD region, that is, the bulk Cu deposition and its subsequent stripping is avoided (see Supplementary Figure 1). In addition, the response of the polyoriented Pd surface is multiplied by an arbitrary number to better correlate their different contributions with those obtained with the Pd basal electrodes. The results obtained are in agreement with those previously reported in the literature (Chierchie and Mayer, 1988; Rigano et al., 1990; Cuesta et al., 1999; Okada et al., 2001). For the Pd(111) electrode, well-defined anodic and cathodic peaks at 0.53 and 0.50 V are observed, respectively. The Cu UPD on Pd(110) is much more



complex and, in the anodic region, displays wide features at 0.56 and 0.58 V. Also a couple of contributions at 0.40 and 0.43 V are observed related to the Cu UPD second layer deposition on Pd(110). Finally, the Cu UPD response on Pd(100) again shows well-defined anodic and cathodic peaks, in this case at 0.55 and 0.52 V, respectively. However, and due to some surface imperfections/defects, some small contributions at the potentials corresponding to the other basal planes are also visible. Interestingly, the Cu UPD response on the polyoriented Pd electrode is essentially similar to that previously reported by Chierchie and Mayer (1988) and contains multiple contributions which can be well-correlated with the signals previously observed with the Pd single crystal basal planes. Thus, in the positive going sweep, voltammetric features related to {111} (peak at about 0.52 V), {100} (peak at about 0.55 V), and {110} (multiple contributions between 0.40–0.45 and 0.56–0.66 V) surface domains are evident. Also, some additional contributions can be observed between 0.30 and 0.33 V which were previously related to the second Cu monolayer on {100} surface domains (Cuesta et al., 1999; Vidal-Iglesias et al., 2006). Similar Cu UPD voltammetric profiles can be observed with Pd single crystal electrodes prepared by the “forced deposition” method followed by flame annealing of Pd on Pt single crystal electrodes (Vidal-Iglesias et al., 2006, 2007) (see **Supplementary Figure 2**). **Table 2** recompiles the main features [peak position and full width at half maximum (FWHM)] obtained in **Figure 4** with the three palladium basal planes.

The Cu UPD voltammetric profiles obtained with the Pd_{Cub}, Pd_{Oct}, and Pd_{RD} nanoparticles are reported in **Figure 5**. Assuming that these shaped Pd nanoparticles will have a preferential {100}, {111}, and {110} surface structure, the Cu UPD response of the corresponding Pd basal planes is also included for the sake of comparison. The results clearly demonstrated that, as expected, the cubic, octahedral and rhombic dodecahedra Pd nanoparticles show a preferential {100}, {111}, and {110} surface structure. However, it is worth noting that the Cu UPD voltammetric features observed with the nanoparticles are

broader as a consequence of the presence of domains with different terrace widths. In addition, some minor contributions due to the surface defects including truncations, steps, edges, etc. are also observed. For instance, in case of the Pd_{Oct}, some features related to {110} contributions are visible between 0.56 and 0.65 V.

Once qualitatively demonstrated that the shaped Pd nanoparticles present a preferential surface structure according with their particle shape, the objective is evaluating if this Cu UPD can also provide quantitative information about the {100}, {111}, and {110} surface domains present at the surface of each type of nanoparticles. With this objective in mind, the Cu UPD voltammetric profiles have been fitted using pseudo-Voigt functions located at the characteristic contributions of the {100}, {110}, and {111} surface domains previously obtained from the Pd single crystal experiments and reported in **Figure 4**. The percentages of {100}, {110}, and {111} surface sites have been calculated from the area of each corresponding signal in relation to the total area of the Cu UPD process. However, certain questions must be taken into consideration in order to carry out this calculation correctly. Firstly, the contributions between ~ 0.3 and ~0.5 V cannot be used in the analysis because it is accepted they are related to the formation of a second Cu layer on Pd(100) and Pd(110), respectively (Chierchie and Mayer, 1988; Cuesta et al., 1999; Vidal-Iglesias et al., 2006). Secondly, due to the fact that for the three Pd basal planes the area corresponding to Cu UPD process is different, the area of the different contributions between 0.5 and 0.75 V must be also normalized by considering the calculated charges for a complete Cu monolayer on Pd(111), Pd(100), and Pd(110) single crystals (486, 421, and 297 $\mu\text{C cm}^{-2}$, respectively) (Cuesta et al., 1999; Solla-Gullon et al., 2015). Therefore, and using as normalization value the charge for a complete Cu monolayer on a Pd(110) electrode, the contributions related to the {111} and {100} must be divided by 1.64 (486/297) and 1.42 (421/297), respectively. **Figure 6** shows the deconvolution of the Cu UPD curves shown in **Figure 5**. In all cases, the cumulative curve fits well with the experimental one. **Table 3** summarizes the main results of this deconvolution process. It is worth noting that in the case of the octahedral Pd nanoparticles (**Figure 6B**), the main contribution centered at 0.53 V is, in fact, composed of two very close but discernible contributions. This feature which is not observed on Pd(111), may suggest the presence of a bimodal distribution of {111} surface domains.

The results included in **Table 3** are in reasonably good agreement with the statistic obtained from the TEM analysis [cubes (96.0%), octahedra (89.1%), and rhombic dodecahedra (93.3%)]. For the cubic Pd nanoparticles, the deconvolution indicates that these present an 81% of {100} domains and a 9 and 10% of {111} and {110} sites, respectively. The octahedral ones show a 77.3% of {111} domains and a 4.5 and 18.2% of {100} and {110} sites, respectively. Finally, the rhombic dodecahedral Pd nanoparticles display a 70.2% of {110} domains and a 24.8 and 5% of {111} and {100} sites, respectively. As expected, the % of preferential surface sites is lower than the % of preferential shapes. In this sense, it is worth remarking that the surface of the nanoparticles, even

TABLE 3 | Main results of the deconvolution process of the Cu UPD voltammograms on Pd_{Cub}, Pd_{Oct}, and Pd_{RD} nanoparticles shown in **Figure 6**.

	{111} domains	{100} domains	{110} domains	% main shape/TEM
Pd _{Cub}	1 peak	1 peak	1 peak	96
Peak position/V	0.511	0.547	0.591	
FWHM/mV	35	21	39	
% domain	9.0	81.0	10.0	
Pd _{Oct}	1 peak and shoulder	1 peak	2 peaks	89
Peak position/V	0.522 and 0.534	0.557	0.575 and 0.607	
FWHM/mV	21 and 18	30	51 and 31	
% domain	54.8 and 22.5	4.5	14.0 and 4.2	
Pd _{RD}	1 peak	1 peak	1 peak	93
Peak position/V	0.531	0.558	0.589	
FWHM/mV	62	31	41	
% domain	24.8	5.0	70.2	

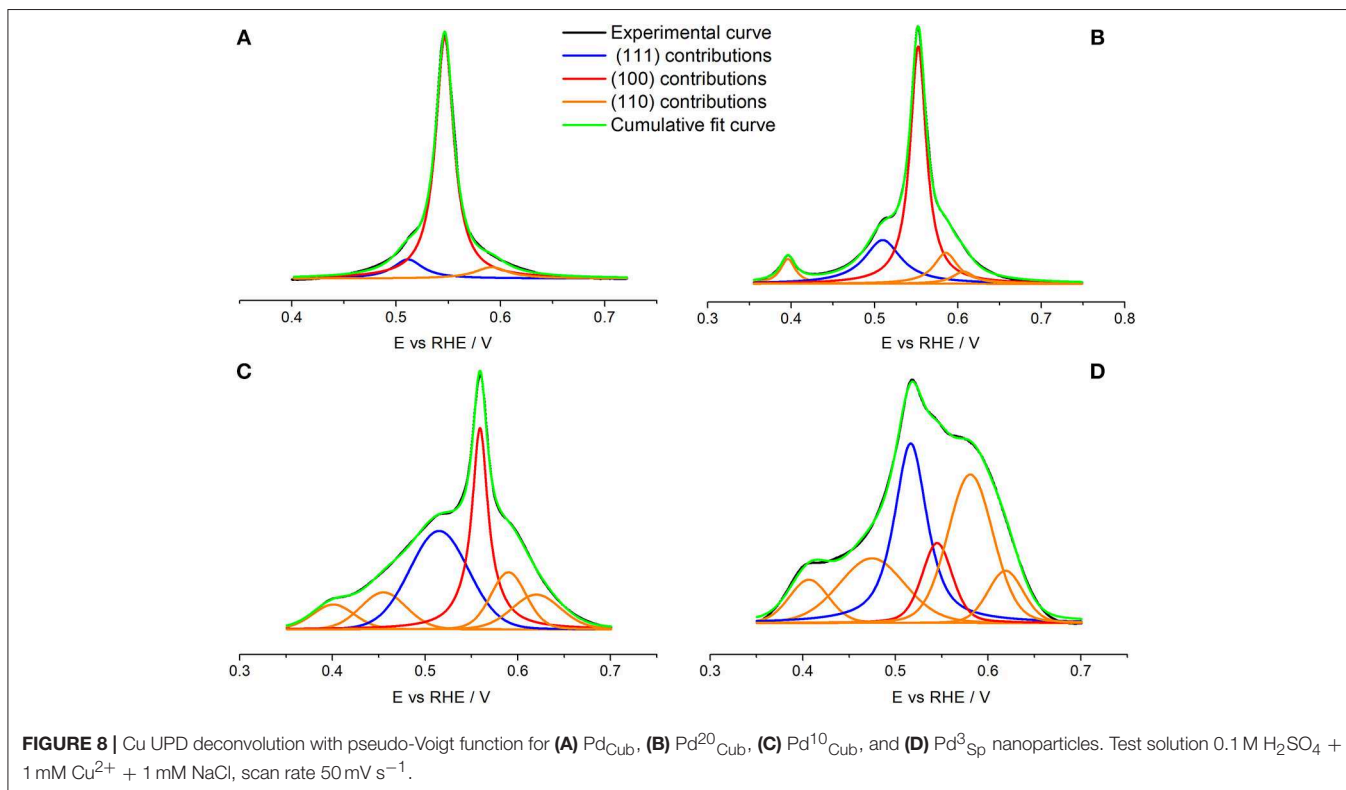
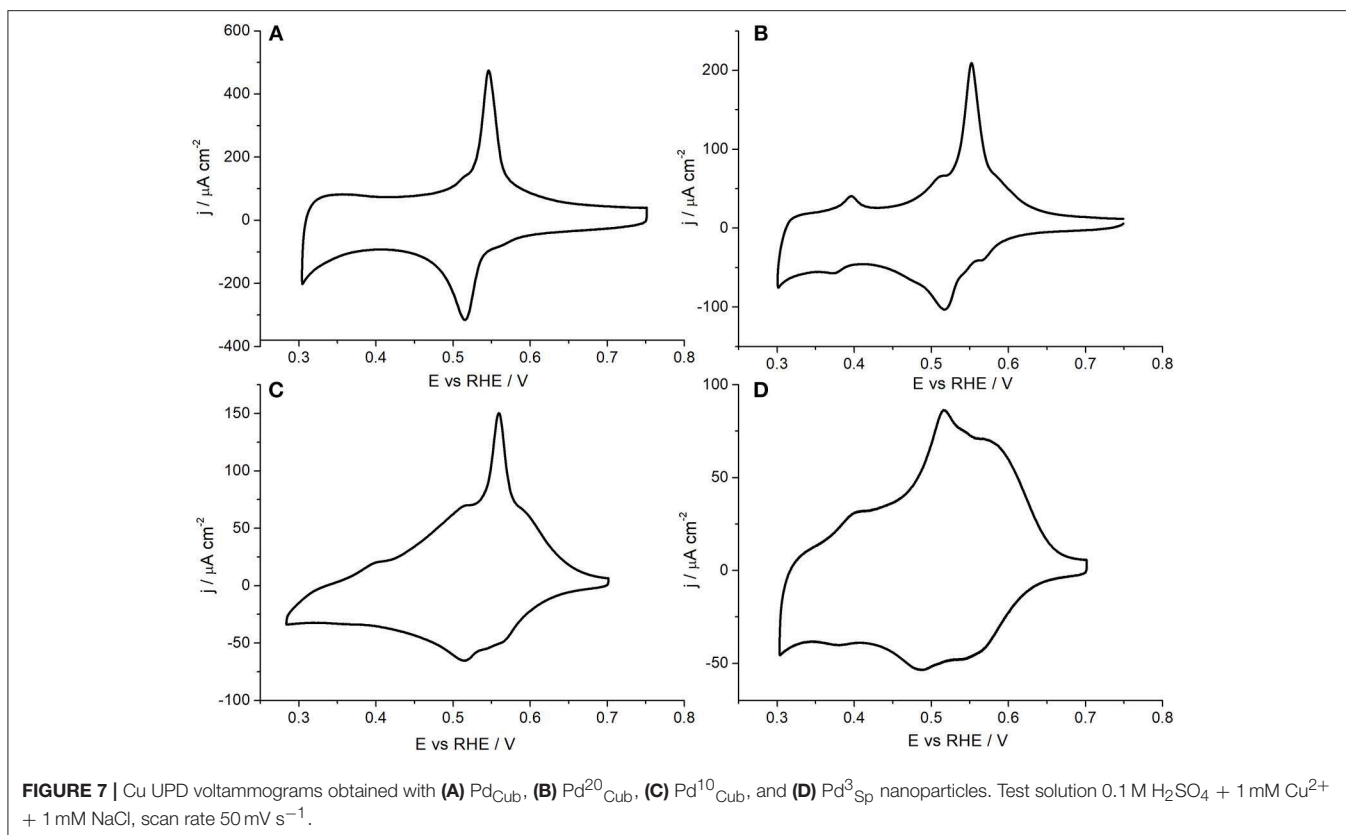


TABLE 4 | Main results of the deconvolution process of the Cu UPD voltammograms on (a) Pd_{Cub}, (b) Pd²⁰_{Cub}, (c) Pd¹⁰_{Cub}, and (d) Pd³_{Sp} nanoparticles shown in **Figure 8**.

	{111} domains	{100} domains	{110} domain	% main shape/TEM
Pd _{Cub}	1 peak	1 peak	1 peak	96
Peak position/V	0.511	0.547	0.591	
FWHM/mV	35	21	39	
% domain	9	81.0	10.0	
Pd ²⁰ _{Cub}	1 peak	1 peak	2 peaks	91.9
Peak position/V	0.510	0.552	0.585 and 0.607	
FWHM/mV	53	23	31 and 57	
% domain	21.0	57.4	15.9 and 5.7	
Pd ¹⁰ _{Cub}	1 peak	1 peak	2 peaks	92.6
Peak position/V	0.515	0.559	0.590 and 0.620	
FWHM/mV	75	22	45 and 62	
% domain	32.2	32.9	19.0 and 15.9	
Pd ³ _{Sp}	1 peak	1 peak	2 peaks	100
Peak position/V	0.516	0.545	0.581 and 0.619	
FWHM/mV	42	39	58 and 62	
% domain	30.4	12.3	44.9 and 12.4	

nanoparticles with a well-defined particle shape, is not perfect and will also contain a considerable amount of surface defects (steps, edges, corners, kinks) which also including concave and convex domains or rounded and truncated corners. This is also supported by the much wider full width at half maximum (FWHM) of the peaks compared to that obtained for the single crystals.

The effect of particle sizes has been previously studied for many electrochemical reactions (Kinoshita, 1990; Shao et al., 2011a). This type of study is particularly interesting in shaped nanoparticles, for which a decrease in their particle size may produce a significant decrease in their preferential surface structure. For example, cubic particles of different sizes have been used for oxygen reduction, and glucose and formic acid oxidations (Erikson et al., 2011, 2016a; Shao et al., 2011b, 2013a; Vidal-Iglesias et al., 2012; Lüsi et al., 2016; Ye et al., 2016; Vara et al., 2017). **Figure 7** shows the Cu UPD voltammetric profiles obtained with the sized controlled cubic Pd nanoparticles (~80, 20, and 10 nm) prepared in this work together with that of the spherical (~3 nm) Pd nanoparticles. The reported results show how the preferential {100} surface structure, associated with the peak at about 0.55 V is, although clearly visible, qualitatively less preferential for decreasing particle sizes. Thus, by decreasing the size, the signals attributed to other surface domains become systematically more perceptible. Finally, for the spherical (~3 nm) Pd nanoparticles, the signal related to the {100} surface site is hardly discernible. To quantitatively evaluate this loss of preferential {100} for decreasing particle size, the Cu UPD responses were deconvoluted as previously discussed in **Figure 6**. These results are shown in **Figure 8** and the main results are summarized in **Table 4**.

The results obtained show that the % of {100} surface domains decreases from 81% to 57 and then to 33% for decreasing particle

sizes from 80 to 20 nm and then to 10 nm, respectively. However, from the TEM statistic, the fraction of cubes was always higher than the 90%. This finding again points out that, for decreasing particle sizes, the contribution of low-coordinated Pd atoms such as edges or corners will represent a larger percentage of the nanoparticles' surface. Obviously, the particular % of surface domains will be strongly affected by the method used for the synthesis, that is, nanoparticles with similar shape and size may have a different % of surface sites as a function of the "quality" of their surface. Finally, the spherical Pd nanoparticles shows a polyoriented surface containing a 57.3% of {110} sites and a 30.4 and 12.3% of {111} and {100} sites, respectively. In summary, the results here reported clearly indicate that Cu UPD is a valuable tool to get insights of the surface structure of different Pd nanoparticles including shape and size-controlled ones.

CONCLUSIONS

In this work, we have demonstrated that Cu UPD is a powerful tool to qualitatively and quantitatively analyse the surface structure of different shape and size controlled Pd nanoparticles. The detailed knowledge of the surface structure of these Pd nanoparticles is particularly important to understand and compare the electrocatalytic activity of these nanomaterials toward relevant surface structure sensitive reactions such as oxygen and CO₂ reduction or the oxidation of small organic molecules, among many others. The Cu UPD results clearly show that the cubic, octahedral and rhombic dodecahedral Pd nanoparticles prepared using the seed-mediated method present a preferential {100}, {111}, and {110} surface structure, respectively, with percentages of the corresponding domains higher than the 70% in all cases. On the other hand, for the size-controlled Pd nanocubes, the decrease of the particle size produces an evident loss of the {100} quality of the Pd nanocubes despite the fraction of cubes, as deduced from the TEM statistic, remains higher than 90%. This finding again evidences that the electrochemical response is determined by the surface structure but not by the shape or size of the particle.

DATA AVAILABILITY

The datasets generated for this study are available on request to the corresponding author.

AUTHOR CONTRIBUTIONS

EG, FV-I, and JS-G carried out the synthesis, characterization, and electrochemical analysis of the Pd samples. JF and JS-G supervised the work. All authors contributed to write and revise the manuscript.

ACKNOWLEDGMENTS

This work was conducted under the framework of the Spanish Ministry of Economy, Industry and Competitiveness (MINECO),

projects CTQ2016-76231-C2-2-R (AEI/FEDER, UE) and CTQ2016-76221-P (AEI/FEDER, UE). JS-G acknowledges financial support from VITC (Vicerrectorado de Investigación y Transferencia de Conocimiento) of the University of Alicante (UATALENTO16-02).

REFERENCES

- Arjona, N., Guerra-Balcázar, M., Ortiz-Frade, L., Osorio-Monreal, G., Álvarez-Contreras, L., Ledesma-García, J., et al. (2013). Electrocatalytic activity of well-defined and homogeneous cubic-shaped Pd nanoparticles. *J. Mater. Chem. A* 1, 15524–15529. doi: 10.1039/C3TA13891G
- Burke, L. D., and Nagle, L. C. (1999). Anomalous electrochemical behaviour of palladium in aqueous solution. *J. Electroanal. Chem.* 461, 52–64. doi: 10.1016/S0022-0728(98)00065-5
- Chen, J., Mao, J., Zhao, J., Ren, M., and Wei, M. (2014). Surfactant-free platinum nanocubes with greatly enhanced activity towards methanol/ethanol electrooxidation. *RSC Adv.* 4, 28832–28835. doi: 10.1039/c4ra03446e
- Chen, Q. S., Vidal-Iglesias, F. J., Solla-Gullón, J., Sun, S. G., and Feliu, J. M. (2012). Role of surface defect sites: from Pt model surfaces to shape-controlled nanoparticles. *Chem. Sci.* 3, 136–147. doi: 10.1039/C1SC00503K
- Chen, Y., Milenkovic, S., and Hassel, A. W. (2017). {110}-Terminated square-shaped gold nanoplates and their electrochemical surface reactivity. *Chemelectrochem* 4, 557–564. doi: 10.1002/celec.201600307
- Chierchie, T., and Mayer, C. (1988). Voltammetric study of the underpotential deposition of copper on polycrystalline and single crystal palladium surfaces. *Electrochim. Acta* 33, 341–345.
- Clavilier, J., Faure, R., Guinet, G., and Durand, R. (1980). Preparation of monocrystalline Pt microelectrodes and electrochemical study of the plane surfaces cut in the direction of the {111} and {110} planes. *J. Electroanal. Chem.* 107, 205–209.
- Cuesta, A., Kibler, L. A., and Kolb, D. M. (1999). A method to prepare single crystal electrodes of reactive metals: application to Pd(hkl). *J. Electroanal. Chem.* 466, 165–168.
- Erikson, H., Lüsü, M., Sarapuu, A., Tammeveski, K., Solla-Gullón, J., and Feliu, J. M. (2016a). Oxygen electroreduction on carbon-supported Pd nanocubes in acid solutions. *Electrochim. Acta* 188, 301–308. doi: 10.1016/j.electacta.2015.11.125
- Erikson, H., Sarapuu, A., Solla-Gullón, J., and Tammeveski, K. (2016b). Recent progress in oxygen reduction electrocatalysis on Pd-based catalysts. *J. Electroanal. Chem.* 780, 327–336. doi: 10.1016/j.jelechem.2016.09.034
- Erikson, H., Sarapuu, A., Tammeveski, K., Solla-Gullón, J., and Feliu, J. M. (2011). Enhanced electrocatalytic activity of cubic Pd nanoparticles towards the oxygen reduction reaction in acid media. *Electrochem. Commun.* 13, 734–737. doi: 10.1016/j.elecom.2011.04.024
- Fang, L. L., Tao, Q., Li, M. F., Liao, L. W., Chen, D., and Chen, Y. X. (2010). Determination of the real surface area of palladium electrode. *Chin. J. Chem. Phys.* 23, 543–548. doi: 10.1088/1674-0068/23/05/543-548
- Farias, M. J. S., and Feliu, J. M. (2019). Determination of specific electrocatalytic sites in the oxidation of small molecules on crystalline metal surfaces. *Top. Curr. Chem.* 377:5. doi: 10.1007/s41061-018-0228-x
- Figueiredo, M. C., Solla-Gullón, J., Vidal-Iglesias, F. J., Climent, V., and Feliu, J. M. (2013). Nitrate reduction at Pt(100) single crystals and preferentially oriented nanoparticles in neutral media. *Catal. Today* 202, 2–11. doi: 10.1016/j.cattod.2012.02.038
- Gao, D., Zhou, H., Cai, F., Wang, J., Wang, G., and Bao, X. (2018). Pd-Containing nanostructures for electrochemical CO₂ reduction reaction. *ACS Catal.* 8, 1510–1519. doi: 10.1021/acscatal.7b03612
- García-Cruz, L., Montiel, V., and Solla-Gullón, J. (2019). Shape-controlled metal nanoparticles for electrocatalytic applications. *Phys. Sci. Rev.* 4:20170124. doi: 10.1515/psr-2017-0124
- Hara, M., Linke, U., and Wandlowski, T. (2007). Preparation and electrochemical characterization of palladium single crystal electrodes in 0.1 M H₂SO₄ and HClO₄ part I. Low-index phases. *Electrochim. Acta* 52, 5733–5748. doi: 10.1016/j.electacta.2006.11.048
- Hernández, J., Solla-Gullón, J., Herrero, E., Feliu, J. M., and Aldaz, A. (2009). *In situ* surface characterization and oxygen reduction reaction on shape-controlled gold nanoparticles. *J. Nanosci. Nanotechnol.* 9, 2256–2273. doi: 10.1166/jnn.2009.SE38
- Herrero, E., Buller, L. J., and Abruna, H. D. (2001). Underpotential deposition at single crystal surfaces of Au, Pt, Ag and other materials. *Chem. Rev.* 101, 1897–1930. doi: 10.1021/cr9600363
- Higuchi, E., Kawai, M., Chiku, M., and Inoue, H. (2018). Synthesis and electrochemical characterization of palladium crystals enclosed by (100) facets by seed-mediated fabrication. *Int. J. Electrochem.* 2018:6. doi: 10.1155/2018/7138638
- Hoshi, N., Kagaya, K., and Hori, Y. (2000). Voltammograms of the single-crystal electrodes of palladium in aqueous sulfuric acid electrolyte: Pd(S)-[n(111)x(111)] and Pd(S)-[n(100)x(111)]. *J. Electroanal. Chem.* 485, 55–60. doi: 10.1016/S0022-0728(00)00098-X
- Hoshi, N., Kuroda, M., and Hori, Y. (2002). Voltammograms of stepped and kinked stepped surfaces of palladium: Pd(S)-[n(111) x (100)] and Pd(S)-[n(100) x (110)]. *J. Electroanal. Chem.* 521, 155–160. doi: 10.1016/S0022-0728(02)00687-3
- Huang, H., Jia, H., Liu, Z., Gao, P., Zhao, J., Luo, Z., et al. (2017). Understanding of strain effects in the electrochemical reduction of CO₂: using Pd nanostructures as an ideal platform. *Angew. Chem. Int. Ed.* 56, 3594–3598. doi: 10.1002/anie.201612617
- Jeyabharathi, C., Zander, M., and Scholz, F. (2018). Underpotential deposition of lead on quasi-spherical and faceted gold nanoparticles. *J. Electroanal. Chem.* 819, 159–162. doi: 10.1016/j.jelechem.2017.10.011
- Jin, M., Zhang, H., Xie, Z., and Xia, Y. (2012). Palladium nanocrystals enclosed by {100} and {111} facets in controlled proportions and their catalytic activities for formic acid oxidation. *Energy Environ. Sci.* 5, 6352–6357. doi: 10.1039/C2EE02866B
- Kannan, P., Maiyalagan, T., and Opallo, M. (2013). One-pot synthesis of chain-like palladium nanocubes and their enhanced electrocatalytic activity for fuel-cell applications. *Nano Energy* 2, 677–687. doi: 10.1016/j.nanoen.2013.08.001
- Kinoshita, K. (1990). Particle size effects for oxygen reduction on highly dispersed platinum in acid electrolytes. *J. Electrochem. Soc.* 137, 845–848.
- Klinkova, A., De Luna, P., Dinh, C.-T., Voznyy, O., Larin, E. M., Kumacheva, E., et al. (2016). Rational design of efficient palladium catalysts for electroreduction of carbon dioxide to formate. *ACS Catal.* 6, 8115–8120. doi: 10.1021/acscatal.6b01719
- Korzeniewski, C., Climent, V., and Feliu, J. (2012). “Electrochemistry at platinum single crystal electrodes,” in *Electroanalytical Chemistry A Series of Advances*, Vol. 24, eds A. J. Bard and C. Zoski (Boca Raton, FL: CRC Press), 75–170.
- Lim, B., Kobayashi, H., Camargo, P. H. C., Allard, L. F., Liu, J., and Xia, Y. (2010). New insights into the growth mechanism and surface structure of palladium nanocrystals. *Nano Res.* 3, 180–188. doi: 10.1007/s12274-010-1021-5
- Long, R., Zhou, S., Wiley, B. J., and Xiong, Y. (2014). Oxidative etching for controlled synthesis of metal nanocrystals: atomic addition and subtraction. *Chem. Soc. Rev.* 43, 6288–6310. doi: 10.1039/c4cs00136b
- Lüsü, M., Erikson, H., Sarapuu, A., Tammeveski, K., Solla-Gullón, J., and Feliu, J. M. (2016). Oxygen reduction reaction on carbon-supported palladium nanocubes in alkaline media. *Electrochem. Commun.* 64, 9–13. doi: 10.1016/j.elecom.2015.12.016
- Mayet, N., Servat, K., Kokoh, K. B., and Napporn, T. W. (2019). Probing the surface of noble metals electrochemically by underpotential deposition of transition metals. *Surfaces* 2, 257–276. doi: 10.3390/surfaces2020020
- Moniri, S., Van Cleve, T., and Linic, S. (2017). Pitfalls and best practices in measurements of the electrochemical surface area of platinum-based nanostructured electro-catalysts. *J. Catal.* 345, 1–10. doi: 10.1016/j.jcat.2016.11.018.

SUPPLEMENTARY MATERIAL

The Supplementary Material for this article can be found online at: <https://www.frontiersin.org/articles/10.3389/fchem.2019.00527/full#supplementary-material>

- Montiel, M. A., Vidal-Iglesias, F. J., Montiel, V., and Solla-Gullón, J. (2017). Electrocatalysis on shape-controlled metal nanoparticles: progress in surface cleaning methodologies. *Curr. Opin. Electrochem.* 1, 34–39. doi: 10.1016/j.coelec.2016.12.007
- Niu, W., Li, Z. Y., Shi, L., Liu, X., Li, H., Han, S., et al. (2008). Seed-mediated growth of nearly monodisperse palladium nanocubes with controllable sizes. *Cryst. Growth Design* 8, 4440–4444. doi: 10.1021/cg8002433
- Niu, W., Zhang, L., and Xu, G. (2010). Shape-controlled synthesis of single-crystalline palladium nanocrystals. *ACS Nano* 4, 1987–1996. doi: 10.1021/nn100093y
- Okada, J., Inukai, J., and Itaya, K. (2001). Underpotential and bulk deposition of copper on Pd(111) in sulfuric acid solution studied by in situ scanning tunneling microscopy. *Phys. Chem. Chem. Phys.* 3, 3297–3302. doi: 10.1039/b101093j
- Rigano, P. M., Mayer, C., and Chierchie, T. (1990). Structural investigation of the initial stages of copper electrodeposition on polycrystalline and single crystal palladium electrodes. *Electrochim. Acta* 35, 1189–1194. doi: 10.1016/0013-4686(90)80038-p
- Rodríguez, P., Herrero, E., Solla-Gullón, J., Vidal-Iglesias, F. J., Aldaz, A., and Feliu, J. M. (2005). Specific surface reactions for identification of platinum surface domains - surface characterization and electrocatalytic tests. *Electrochim. Acta* 50, 4308–4317. doi: 10.1016/j.electacta.2005.02.087
- Scardi, P., Leonardi, A., Gelisio, L., Suchomel, M. R., Sneed, B. T., Sheehan, M. K., et al. (2015). Anisotropic atom displacement in Pd nanocubes resolved by molecular dynamics simulations supported by x-ray diffraction imaging. *Phys. Rev. B* 91:155414. doi: 10.1103/PhysRevB.91.155414
- Shao, M., Odell, J., Humbert, M., Yu, T., and Xia, Y. (2013a). Electrocatalysis on shape-controlled palladium nanocrystals: oxygen reduction reaction and formic acid oxidation. *J. Phys. Chem. C* 117, 4172–4180. doi: 10.1021/jp312859x
- Shao, M., Odell, J. H., Choi, S. I., and Xia, Y. (2013b). Electrochemical surface area measurements of platinum- and palladium-based nanoparticles. *Electrochem. Commun.* 31, 46–48. doi: 10.1016/j.elecom.2013.03.011
- Shao, M., Peles, A., and Shoemaker, K. (2011a). Electrocatalysis on platinum nanoparticles: particle size effect on oxygen reduction reaction activity. *Nano Lett.* 11, 3714–3719. doi: 10.1021/nl2017459
- Shao, M., Yu, T., Odell, J. H., Jin, M., and Xia, Y. (2011b). Structural dependence of oxygen reduction reaction on palladium nanocrystals. *Chem. Commun.* 47, 6566–6568. doi: 10.1039/C1CC11004G
- Solla-Gullón, J., Garnier, E., Feliu, J. M., Leoni, M., Leonardi, A., and Scardi, P. (2015). Structure and morphology of shape-controlled Pd nanocrystals. *J. Appl. Crystallogr.* 48, 1534–1542. doi: 10.1107/S1600576715015964
- Solla-Gullón, J., Rodríguez, P., Herrero, E., Aldaz, A., and Feliu, J. M. (2008a). Surface characterization of platinum electrodes. *Phys. Chem. Chem. Phys.* 10, 1359–1373. doi: 10.1039/b709809j
- Solla-Gullón, J., Vidal-Iglesias, F. J., and Feliu, J. M. (2011). Shape dependent electrocatalysis. *Ann. Rep. Prog. Chem. C* 107, 263–297. doi: 10.1039/C1PC90010B
- Solla-Gullón, J., Vidal-Iglesias, F. J., Herrero, E., Feliu, J. M., and Aldaz, A. (2006). CO monolayer oxidation on semi-spherical and preferentially oriented (100) and (111) platinum nanoparticles. *Electrochem. Commun.* 8, 189–194. doi: 10.1016/j.elecom.2005.11.008
- Solla-Gullón, J., Vidal-Iglesias, F. J., López-Cudero, A., Garnier, E., Feliu, J. M., and Aldaz, A. (2008b). Shape-dependent electrocatalysis: methanol and formic acid electrooxidation on preferentially oriented Pt nanoparticles. *Phys. Chem. Chem. Phys.* 10, 3689–3698. doi: 10.1039/b802703j
- Solla-Gullón, J., Vidal-Iglesias, F. J., Rodríguez, P., Herrero, E., Feliu, J. M., Clavilier, J., et al. (2004). In situ surface characterization of preferentially oriented platinum nanoparticles by using electrochemical structure sensitive adsorption reactions. *J. Phys. Chem. B* 108, 13573–13575. doi: 10.1021/jp0471453
- Tian, N., Zhou, Z.-Y., Sun, S.-G., Ding, Y., and Wang, Z. L. (2007). Synthesis of tetrahedral platinum nanocrystals with high-index facets and high electro-oxidation activity. *Science* 316, 732–735. doi: 10.1126/science.1140484
- Tian, N., Zhou, Z. Y., and Sun, S. G. (2008). Platinum metal catalysts of high-index surfaces: from single-crystal planes to electrochemically shape-controlled nanoparticles. *J. Phys. Chem. C* 112, 19801–19817. doi: 10.1021/jp804051e
- Vara, M., Lu, P., Yang, X., Lee, C. T., and Xia, Y. (2017). A photochemical, room-temperature, and aqueous route to the synthesis of Pd nanocubes enriched with atomic steps and terraces on the side faces. *Chem. Mater.* 29, 4563–4571. doi: 10.1021/acs.chemmater.7b01287
- Vidal-Iglesias, F. J., Al Akl, A., Watson, D. J., and Attard, G. A. (2006). A new method for the preparation of PtPd alloy single crystal surfaces. *Electrochem. Commun.* 8, 1147–1150. doi: 10.1016/j.elecom.2006.05.008
- Vidal-Iglesias, F. J., Al-Akl, A., Watson, D., and Attard, G. A. (2007). Electrochemical characterization of PtPd alloy single crystal surfaces prepared using Pt basal planes as templates. *J. Electroanal. Chem.* 611, 117–125. doi: 10.1016/j.jelechem.2007.08.005
- Vidal-Iglesias, F. J., Arán-Ais, R. M., Solla-Gullón, J., Garnier, E., Herrero, E., Aldaz, A., et al. (2012). Shape-dependent electrocatalysis: formic acid electrooxidation on cubic Pd nanoparticles. *Phys. Chem. Chem. Phys.* 14, 10258–10265. doi: 10.1039/c2cp40992e
- Voiry, D., Chhowalla, M., Gogotsi, Y., Kotov, N. A., Li, Y., Penner, R. M., et al. (2018). Best practices for reporting electrocatalytic performance of nanomaterials. *ACS Nano* 12, 9635–9638. doi: 10.1021/acsnano.8b07700
- Wan, L. J., Suzuki, T., Sashikata, K., Okada, J., Inukai, J., and Itaya, K. (2000). In situ scanning tunneling microscopy of adsorbed sulfate on well-defined Pd(111) in sulfuric acid solution. *J. Electroanal. Chem.* 484, 189–193. doi: 10.1016/S0022-0728(00)00082-6
- Woods, R. (1976). “Chemisorption at electrodes: hydrogen and oxygen on noble metals and their alloys”, in *Electroanalytical Chemistry A series of advances*, Vol. 9, ed A. J. Bard (New York, NY: Marcel Dekker, Inc.), 1–162.
- Xiong, Y., Cai, H., Wiley, B. J., Wang, J., Kim, M. J., and Xia, Y. (2007). Synthesis and mechanistic study of palladium nanobars and nanorods. *J. Am. Chem. Soc.* 129, 3665–3675. doi: 10.1021/ja0688023
- Xiong, Y., and Xia, Y. (2007). Shape-controlled synthesis of metal nanostructures: the case of palladium. *Adv. Mater.* 19, 3385–3391. doi: 10.1002/adma.200701301
- Ye, J. S., Hsu, S. Y., and Lee, C. L. (2016). Sequential and transient electrocatalysis of glucose oxidation reactions by octahedral, rhombic dodecahedral, and cubic palladium nanocrystals. *Electrochim. Acta* 211, 1024–1032. doi: 10.1016/j.electacta.2016.06.132
- Yu, N.-F., Tian, N., Zhou, Z.-Y., Sheng, T., Lin, W.-F., Ye, J.-Y., et al. (2019). Pd nanocrystals with continuously tunable high-index facets as a model nanocatalyst. *ACS Catal.* 9, 3144–3152. doi: 10.1021/acscatal.8b04741
- Zalineaeva, A., Baranton, S., and Coutanceau, C. (2013). Bi-modified palladium nanocubes for glycerol electrooxidation. *Electrochem. Commun.* 34, 335–338. doi: 10.1016/j.elecom.2013.07.022
- Zalineaeva, A., Baranton, S., Coutanceau, C., and Jerkiewicz, G. (2015). Electrochemical behavior of unsupported shaped palladium nanoparticles. *Langmuir* 31, 1605–1609. doi: 10.1021/la5025229
- Zhang, H., Jin, M., Xiong, Y., Lim, B., and Xia, Y. (2013). Shape-controlled synthesis of Pd nanocrystals and their catalytic applications. *Acc. Chem. Res.* 46, 1783–1794. doi: 10.1021/ar300209w
- Zhang, J., Zhang, L., Xie, S., Kuang, Q., Han, X., Xie, Z., et al. (2011). Synthesis of concave palladium nanocubes with high-index surfaces and high electrocatalytic activities. *Chem. Eur. J.* 17, 9915–9919. doi: 10.1002/chem.201100868
- Zhou, Z.-Y., Tian, N., Huang, Z.-Z., Chen, D.-J., and Sun, S.-G. (2009). Nanoparticle catalysts with high energy surfaces and enhanced activity synthesized by electrochemical method. *Faraday Discuss.* 140, 81–92. doi: 10.1039/B803716G

Conflict of Interest Statement: The authors declare that the research was conducted in the absence of any commercial or financial relationships that could be construed as a potential conflict of interest.

Copyright © 2019 Garnier, Vidal-Iglesias, Feliu and Solla-Gullón. This is an open-access article distributed under the terms of the Creative Commons Attribution License (CC BY). The use, distribution or reproduction in other forums is permitted, provided the original author(s) and the copyright owner(s) are credited and that the original publication in this journal is cited, in accordance with accepted academic practice. No use, distribution or reproduction is permitted which does not comply with these terms.